Available online at www.sciencedirect.com
ScienceDirect
International Journal of Heat and Mass Transfer 50 (2007) 3340–3350
International Journal of HEAT and MASS TRANSFER
www.elsevier.com/locate/ijhmt

Entrance effect on heat transfer to laminar flow through passages

A. Haji-Sheikh [a,*], J.V. Beck [b]

[a] Department of Mechanical and Aerospace Engineering, The University of Texas at Arlington, Arlington, TX 76019-0023, USA
[b] Department of Mechanical Engineering, Michigan State University, East Lansing, MI 48824-1226, USA

Received 4 January 2007; received in revised form 26 January 2007
Available online 28 March 2007

Abstract

This paper presents an accurate methodology to determine heat transfer coefficients near the thermal entrance region of ducts. These include parallel plate channels, circular pipes and rectangular passages. The solution technique uses a classical Airy differential equation when the thermal penetration is small. The validation and verification of these solutions are the essential part of this presentation as they are compared with available solutions. The results show a high degree of accuracy when the thermal entrance distance is very small. Also, this paper discusses the range of validity of this solution since its accuracy reduces at a larger distance from the thermal entrance location.

Keywords: Convection; Heat transfer; Thermal entrance; Parallel plate ducts; Circular pipes

1. Introduction

Solutions for heat transfer with laminar fluid flow in different passages and under different wall conditions are available in the literature [1,2]. Generally, series solutions are used to compute the heat transfer in the thermally developing regions [3–5]. These solutions have a convergence limitation and will not provide sufficient accuracy near the thermal entrance location. Typically, the Nusselt number is known at different values of $(x/D_h)/(Re_D Pr)$ for flow through various ducts where the Prandtl number $Pr = \mu c_p/k$, the Reynolds number $Re_D = \rho U D_h/\mu$, U is the average velocity, and D_h is the hydraulic diameter. The minimum values from available information can provide heat transfer data at small values of (x/D_h) when $Re_D Pr$ is also small but larger than ~10. However, in many applications, the value of $Re_D Pr$ for laminar flow is relatively large and, therefore, it is difficult to obtain the local heat transfer information at small values of (x/D_h). As an example, for rectangular passages, the average Nusselt number is given in [3, Table 9-9] for $(x/D_h)/(Re_D Pr) \geqslant 0.01$. When $Re_D Pr = 500$, these data do not provide adequate information for $(x/D_h) < 5$, an important range for cooling the microelectronic devices. Accordingly, there is a need for a relatively accurate knowledge of heat transfer near the entrance locations; especially, when $Re_D Pr$ is relatively large. It should be noted that the present analysis is restricted to negligible axial conduction but the same concepts have potential for treating axial conduction.

The main objective of this study is to provide a method that yields accurate asymptotic temperature solutions when x is very small. A comparison between this solution and the one obtained by the exact series solution, at larger values of x, validates its accuracy. The following analysis begins by considering the wall to be flat when the thermal penetration distance is small relative to the radius of the curvature of the wall. This makes the heat transfer within a parallel plate channel a primary candidate and the extension of this methodology to other geometries follow in a straightforward manner. Accordingly, this is demonstrated by applying it to circular pipes and then to rectangular ducts.

The physical problem has a very short penetration distance normal to the wall, designated as y. In regions of steep changes followed by negligible penetration, series solutions have great difficulty. This suggests a modified

* Corresponding author. Tel.: +1 817 272 2010; fax.: +1 817 272 2952.
E-mail address: haji@uta.edu (A. Haji-Sheikh).

0017-9310/$ - see front matter © 2007 Elsevier Ltd. All rights reserved.
doi:10.1016/j.ijheatmasstransfer.2007.01.028

Nomenclature

A	area, m^2
a, b	channel dimensions, m
$\bar{b}$	b/a
C	velocity slope, s^{-1}
$\overline{C}$	effective dimensionless slope, see Eq. (35)
C_1, C_2	coefficients
D_h	hydraulic diameter, m
F_n	eigenfunctions
h	local heat transfer coefficient W/m^2 K
$\bar{h}$	average heat transfer coefficient, W/m^2 K
k	thermal conductivity, W/m K
Nu_D	Nusselt number, hD_h/k
$\overline{Nu}_D$	average Nusselt number, $\bar{h}D_h/k$
p	pressure, Pa
Pe	Peclet number, Ua/α or Ur_o/α
Pr	Prandtl number, $\mu c_p/k$
q	heat flux, W/m^2 K
q_w	wall heat flux, W/m^2 K
Re_D	Reynolds number, $\rho UD_h/\mu$
r	radial coordinate
r_o	pipe radius, m
T	temperature, K
T_b	bulk temperature, K
T_i	inlet temperature, at $x = 0$, K
T_w	wall temperature, K
u	velocity, m/s
U	average velocity, m/s
x	axial coordinate, m
$\hat{x}$	$(x/a)/Pe$
y, z	coordinates, m

Greek symbols

α	thermal diffusivity, m^2/s
β_n	eigenvalues in Eq. (31a)
γ	parameter, Eq. (38)
ε	percent deviation, Eq. (20)
θ	$(T - T_i)/(T_w - T_i)$
μ	fluid viscosity, N s/m^2
ρ	density, kg/m^3
Φ	$(T - T_i)/(q_w a/k)$
ψ	coefficient, Eq. (39b)

Subscripts

b	bulk
i	inlet
L	large x
S	small x
w	wall

physical problem and a different method of solution. Since the temperature penetration is so small in the y-direction, the velocity distribution can be modeled as being linear with y. Moreover, the temperature distribution becomes locally a function of just x and y (even for rectangular cross-sections, for example) and the fluid can be modeled as being infinite in the y-direction. This heat transfer problem can be solved in closed form which does not involve infinite series and yet is much more accurate than the series solution as x goes to zero.

2. Analysis using Airy differential equation

This derivation is limited to the case when flow is hydrodynamically fully-developed and axial conduction is negligible. At a very small distant from the thermal entrance location in a duct having a constant wall temperature, the fluid temperature is affected only very near the wall. Therefore, it is appropriate to let the coordinate measured from the wall be denoted y and the coordinate in the direction of flow be denoted x. For the steady state case, the energy equation can be written as

$$\alpha \frac{\partial^2 T}{\partial y^2} = u \frac{\partial T}{\partial x} \tag{1}$$

For points near the wall, the velocity is modeled as being linear with distance from the wall, y. Then, the velocity near the wall can be written as

$$u = Cy, \quad C = \left.\frac{\partial u}{\partial y}\right|_{y=0} \tag{2}$$

For fully-developed flow, Eq. (1) becomes

$$\alpha \frac{\partial^2 T}{\partial y^2} = Cy \frac{\partial T}{\partial x} \tag{3a}$$

For an isothermal wall, the boundary conditions are

$$T(x,0) = T_w, \quad T(0,y) = T_i, \quad T(x,\infty) = T_i \tag{3b}$$

This differential equation is similar to that for heat transfer in Couette flow as discussed in [7]. However, the boundary conditions and the method of solution are different. Kestin and Persen [8] solved a similar problem for turbulent flow when the temperature change is confined within the laminar sublayer. They developed a similarity solution [8, Eq. (13)] and the resulting differential equation was solved. In following formulation, for a small-x solution, the Laplace transform technique reduces the partial differential equation to a classical ordinary differential equation with a known solution.

The next step is to find a solution for Eq. (3a) with boundary condition as given by Eq. (3b). In dimensionless form, let $\theta(x,y) = [T(x,y) - T_i]/(T_w - T_i)$ and this makes

$$\alpha \frac{\partial^2 \theta}{\partial y^2} = Cy \frac{\partial \theta}{\partial x} \tag{4}$$

with boundary conditions of

$$\theta(x,0)=1,\quad \theta(0,y)=0,\quad \theta(x,\infty)=0$$

Now, taking the Laplace transform with respect to x of Eq. (4) results in the relation

$$\alpha\frac{\mathrm{d}^2\bar{\theta}}{\mathrm{d}y^2}=Cys\bar{\theta} \tag{5}$$

where $\bar{\theta}(s,y)$ is the Laplace transform with respect to x of $\theta(x,y)$. To change the variables, let

$$\eta=y\left(\frac{Cs}{\alpha}\right)^{1/3}\quad\text{or}\quad y=\eta\left(\frac{\alpha}{Cs}\right)^{1/3} \tag{6}$$

and then introducing η into Eq. (5) gives

$$\frac{\alpha}{\left(\frac{\alpha}{Cs}\right)^{2/3}}\frac{\mathrm{d}^2\bar{\theta}}{\mathrm{d}\eta^2}=C\eta\left(\frac{\alpha}{Cs}\right)^{1/3}s\bar{\theta} \tag{7}$$

that reduces to

$$\frac{\mathrm{d}^2\bar{\theta}(\eta)}{\mathrm{d}\eta^2}=\eta\bar{\theta}(\eta) \tag{8}$$

and its boundary conditions, as given for Eq. (4), are now

$$\bar{\theta}(0)=\frac{1}{s},\quad \bar{\theta}(\infty)=0 \tag{9}$$

Eq. (8) is recognized to be the Airy ordinary differential equation [6, p. 446]. The general solution of Eq. (8) is

$$\bar{\theta}(\eta)=C_1Ai(\eta)+C_2Bi(\eta) \tag{10}$$

Now, the coefficient $Ai(0)$ is a constant and $Ai(\eta)=0$ as $\eta\to\infty$. Also, since $Bi(\infty)=\infty$, using the condition at $\eta=\infty$ gives $C_2=0$ and from the condition at $\eta=0$, one gets

$$\frac{1}{s}=C_1Ai(0)\quad\text{or}\quad C_1=\frac{1}{sAi(0)} \tag{11}$$

Hence, the solution to Eq. (8) with boundary conditions from Eq. (9) is

$$\bar{\theta}(\eta)=\frac{1}{sAi(0)}Ai(\eta) \tag{12}$$

Now, for the determination of the heat transfer coefficient, the heat flux at the wall is needed, that is

$$\begin{aligned}\bar{q}(0,s)&=-k\frac{\mathrm{d}\bar{T}}{\mathrm{d}y}\bigg|_{y=0}=-\frac{k(T_\mathrm{w}-T_\mathrm{i})}{\left(\frac{\alpha}{Cs}\right)^{1/3}}\frac{\mathrm{d}\bar{\theta}}{\mathrm{d}\eta}\bigg|_{\eta=0}\\&=-\frac{k}{\left(\frac{\alpha}{Cs}\right)^{1/3}}\frac{(T_\mathrm{w}-T_\mathrm{i})}{sAi(0)}\frac{\mathrm{d}Ai}{\mathrm{d}\eta}\bigg|_{\eta=0}\\&=-\frac{k(T_\mathrm{w}-T_\mathrm{i})}{s^{3/2}}\left(\frac{C}{\alpha}\right)^{1/3}\frac{Ai'(0)}{Ai(0)}\end{aligned} \tag{13}$$

Taking the inverse Laplace transform of Eq. (12) yields the same temperature field as that in [8],

$$\theta(y,x)=\frac{\Gamma[1/3,y^3C/(9\alpha x)]}{\Gamma(1/3)} \tag{14a}$$

and the heat flux at the wall after a Laplace transform inversion of Eq. (13) is

$$\begin{aligned}q(0,x)&=-k(T_\mathrm{w}-T_\mathrm{i})\left(\frac{C}{\alpha}\right)^{1/3}\frac{Ai'(0)}{Ai(0)}\frac{x^{-1/3}}{\Gamma(2/3)}\\&=-\frac{k(T_\mathrm{w}-T_\mathrm{i})}{\Gamma(2/3)}\frac{Ai'(0)}{Ai(0)}\left(\frac{C}{\alpha x}\right)^{1/3}\\&=\frac{k(T_\mathrm{w}-T_\mathrm{i})}{\Gamma(1/3)}\left(\frac{3C}{\alpha x}\right)^{1/3}\end{aligned} \tag{14b}$$

In this relation, the parameter C is the slope in the velocity at the wall.

2.1. Application to parallel plate ducts

For flow between parallel plates, the fully-developed velocity distribution is

$$\frac{u}{U}=\frac{3}{2}\left[2\left(\frac{y}{a}\right)-\left(\frac{y}{a}\right)^2\right] \tag{15}$$

where a is the channel half-width. The derivative of u with respect to y and evaluated at $y=0$ is

$$\frac{\mathrm{d}u}{\mathrm{d}y}\bigg|_{y=0}=3\frac{U}{a} \tag{16}$$

and therefore, $C=3U/a$, in this case. Introducing this value of C into Eq. (14b) gives

$$\begin{aligned}q(0,x)&=\frac{k(T_\mathrm{w}-T_\mathrm{i})}{\Gamma(1/3)}\left(\frac{9U}{\alpha a x}\right)^{1/3}\\&=\frac{3^{2/3}}{\Gamma(1/3)}\left(\frac{U}{\alpha a x}\right)^{1/3}k(T_\mathrm{w}-T_\mathrm{i})\end{aligned} \tag{17}$$

The heat transfer coefficient is contained in the heat flux equation,

$$q(0,x)=h(T_\mathrm{w}-T_\mathrm{b})=h(T_\mathrm{w}-T_\mathrm{i})(1-\theta_\mathrm{b}) \tag{18}$$

where T_b is the bulk temperature; for this case at very near the entrance, the bulk temperature T_b or θ_b is nearly equal to zero. Then, equating Eqs. (17) and (18) yields,

$$\frac{3^{2/3}}{\Gamma(1/3)}\left(\frac{U}{\alpha a x}\right)^{1/3}k(T_\mathrm{w}-T_\mathrm{i})=h(T_\mathrm{w}-T_\mathrm{i})(1-\theta_\mathrm{b})$$

and when $\theta_\mathrm{b}\cong 0$, this yields the following expression for the heat transfer coefficient

$$\frac{h(2a)}{k}=\frac{2\times 3^{2/3}}{\Gamma(1/3)}\left(\frac{Ua^2}{\alpha x}\right)^{1/3}=1.5529\left(\frac{Ua^2}{\alpha x}\right)^{1/3} \tag{19a}$$

or

$$Nu_\mathrm{D}=\frac{hD_\mathrm{h}}{k}=\frac{3.106}{(\hat{x})^{1/3}} \tag{19b}$$

since the parameter $(\alpha x)/(Ua^2)$ is designated as $\hat{x}=(x/a)/Pe$ wherein $Pe=(a/D_\mathrm{h})Re_\mathrm{D}Pr$. It is significant that the above analysis relates the heat transfer coefficient to the axial

distance to the −1/3 power; the series solutions do not produce such a simple result.

Now, it is appropriate to compare this solution with the existing Graetz type series solution data in Table 1, as they appear in [9]. As an illustration, when the dimensionless axial coordinate $(x/D_h)/(Re_D Pr) = 0.000005$, the Nusselt number $Nu_D = hD_h/k$ is 71.830 in [9]. Since $D_h = 4a$, for the case of

$$\frac{Ua}{\alpha}\frac{a}{x} = 0.000005\left(\frac{D_h}{a}\right)^2 = 0.00008$$

the value of $Nu_D = 2 \times 36.04 = 72.08$, from Eq. (19b), compares well with 71.83 with a deviation of 0.49%. Next, it is desirable to compare graphically this solution to an exact series solution. Although the convergence of a series solution is demanding at very small values of $\hat{x}$, it can provide solutions with high degrees of accuracy at intermediate values. Fig. 1 provides the percent deviation

$$\varepsilon = \frac{(Nu_D)_S - (Nu_D)_L}{(Nu_D)_L} \times 100\% \tag{20}$$

between the exact series solution designated as $(Nu_D)_L$ and the small-x solution designated as $(Nu_D)_S$. This percent deviation appears as a dash line with diamond-shaped symbols; it is small at small values of $\hat{x}$ and shows a tendency to go toward zero at $\hat{x}$ goes to zero. This small deviation emerges because the linear velocity in Eq. (3a) is slightly larger than the actual velocity within the thermal penetration region. However, there is another small deviation, due to the selection of $\theta_b = 1$, in the opposite direction. Then, it begins to influence the value of Nusselt number and causes a rapid reduction as $\hat{x}$ increases beyond 10^{-4}.

Table 1
Comparison of data from Eqs. (21) and (24) with the exact series solutions of local and average Nusselt numbers for flow through parallel plate channels

$\hat{x}(a/D_h)^2$	Nu_D [9]	Nu_D Eq. (21)	ε Eq. (20)	$\overline{Nu}_D$ [9]	$\overline{Nu}_D$ Eq. (24)	ε Eq. (20)
5E–07	154.26	155.3	0.670	232.76	232.9	0.076
1E–06	122.93	123.3	0.267	184.55	184.9	0.180
2E–06	97.538	97.83	0.303	146.42	146.7	0.221
5E–06	71.830	72.09	0.366	107.83	108.1	0.275
0.00001	56.999	57.23	0.408	85.557	85.83	0.316
0.00002	45.245	45.44	0.437	67.890	68.13	0.357
0.00005	33.379	33.52	0.430	50.027	50.22	0.394
0.0001	26.560	26.66	0.377	39.736	39.90	0.400
0.0002	21.188	21.24	0.268	31.598	31.72	0.372
0.0005	15.830	15.84	0.064	23.416	23.48	0.278
0.001	12.822	12.82	−0.033	18.752	18.79	0.179
0.002	10.545	10.55	0.101	15.125	15.14	0.124
0.005	8.5167	8.580	0.742	11.623	11.66	0.303
0.01	7.7405	7.775	0.450	9.8249	9.875	0.515
0.02	7.5495	7.541	-0.117	8.7133	8.731	0.204
0.05	7.5407	7.541	0.000	8.0103	8.019	0.110
0.10	7.5407	7.541	0.000	7.7755	7.780	0.058
0.20	7.5407	7.541	0.000	7.6581	7.660	0.031
0.50	7.5407	7.541	0.000	7.5877	7.589	0.014
1.00	7.5407	7.541	0.000	7.5642	7.565	0.009

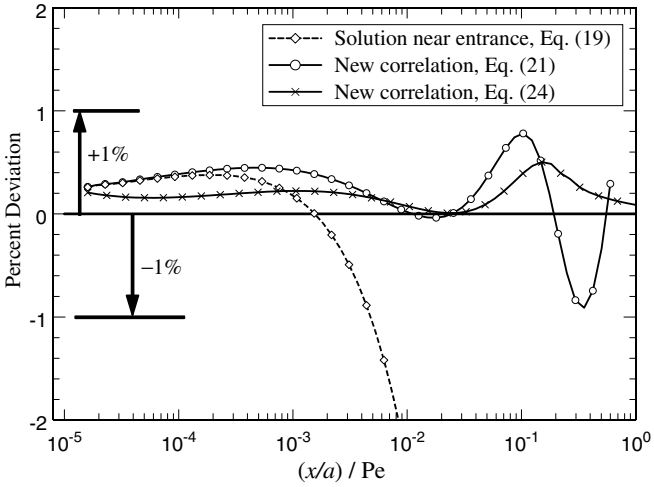

Fig. 1. Percent deviations for near entrances solution, Eq. (19b), and for new correlations for Nu_D, Eq. (21), and $\overline{Nu}_D$, Eq. (23a), as a function of $\hat{x}$ in parallel-plate channels.

This deviation at small x is negligible for parallel plate channels, but become relatively large for other ducts. Fig. 2 compares this solution at a broad range of $\hat{x}$ values with the exact series solution. One can observe that these two solution agree well when $\hat{x}$ is small.

In general, available heat transfer data in the literature, for laminar internal flow, emphasize near thermally fully-developed conditions; the available Nusselt number correlations confirm this trend. To have accurate heat transfer data extending to $\hat{x} = 0$, a correlation for the local Nusselt number is proposed that emphasizes this small-x solution as

$$Nu_D = \frac{hD_h}{k} = \frac{3.106}{(\hat{x})^{1/3}} + \frac{7.541}{\left[1 + 112(\hat{x})^{-0.9}/125\right]^{3/4}}$$
$$\text{for } 0 \leqslant \hat{x} \leqslant 0.25 = 7.541 \quad \text{for } 0.25 < \hat{x} < \infty \tag{21}$$

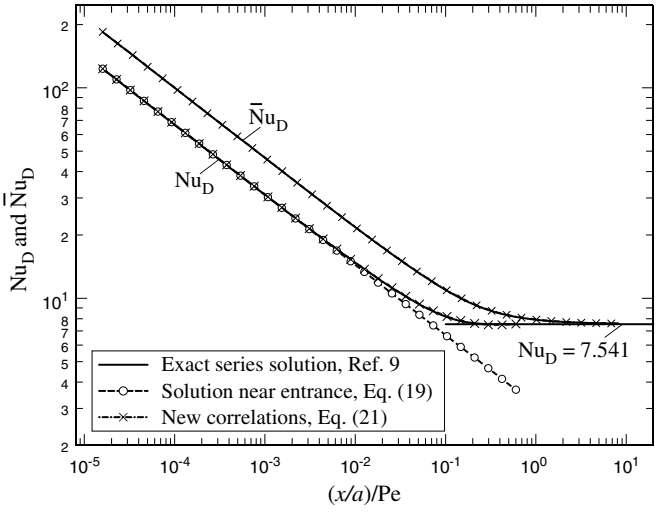

Fig. 2. A comparison of the Nusselt numbers from small-x solution, this new correlation, Eq. (21), and the exact series solution for laminar flow through parallel-plate channels.

This equation is prepared so that the second term would vanish as $\hat{x}$ goes toward zero; therefore, it would not alter the solution given by Eqs. (19a) and (19b) for this condition. Moreover, the second term approaches the thermally fully-developed solution as $\hat{x}$ become large. The solid line with circular symbols in Fig. 1 is the corresponding deviation when the Nusselt number from this correlation, Eq. (21), replaces that for the small-x solution $(Nu_D)_S$ in Eq. (20). Fig. 2 compares these local Nusselt number values from Eqs. (19b) and (21) with those from [9] and the figure indicates graphically indistinguishable differences between this correlation, Eq. (21), and that from the exact series solution [9]. The dash line with circular symbol represents the small-x solution in this figure and, as expected, it agrees well with other data at small values of $\hat{x}$ and it only deviates as $\hat{x}$ becomes larger than 0.01.

Table 1 also presents a sample of data comparing those from Eq. (21) with Column 2 taken from [9]. The deviation ε is generally better than the targeted accuracy of less than 1%. Next, the average Nusselt number $\overline{Nu}_D = \bar{h}D_h/k$ is determined from the equation

$$\overline{Nu}_D = \frac{1}{\hat{x}}\int_0^{\hat{x}} Nu_D \, d\hat{x} \tag{22}$$

Following the substitution of Nu_D from Eq. (21) into Eq. (22), the integration yields

$$\overline{Nu}_D = \frac{4.6587}{\hat{x}^{1/3}} + \frac{2.2553\hat{x}^{-0.9}}{(125+112x^{-0.9})^{3/4}} \times \left\{ 112 + 125\hat{x}^{0.9} - 2.2795(112+125\hat{x}^{0.9})^{3/4} \times {}_2F_1\left[\frac{31}{36}, \frac{3}{4}, \frac{67}{36}, -\frac{125}{112}\hat{x}^{0.9}\right]\right\} \quad \text{when } 0 \leqslant \hat{x} \leqslant 0.25 \tag{23a}$$

and

$$\overline{Nu}_D = 7.541 + 0.381/\hat{x} \quad \text{when } 0.25 < \hat{x} < \infty. \tag{23b}$$

The hypergeometric function ${}_2F_1$ within Eq. (23a) is defined in [6, p. 556]. Table 2 also includes the percent deviation using Eqs. (23a) and (23b) and the data from [9]. It is simpler to use approximate forms of Eqs. (23a) and (23b); with less than 0.6% deviation, they are

$$\overline{Nu}_D = \frac{4.6587}{\hat{x}^{1/3}} + \frac{7.541}{1+1.32\hat{x}^{-0.7}} \quad \text{when } 0 \leqslant \hat{x} \leqslant 0.25$$
$$= 7.541 + \frac{0.381}{\hat{x}} \quad \text{when } 0.25 < \hat{x} < \infty \tag{24}$$

A comparison between the data using Eq. (24) and those from [9] are also in Fig. 2 and the percent deviation is plotted in Fig. 1.

Next, it is desirable to extend this methodology to include passages with different shapes. An excellent candidate for this investigation is the study of heat transfer in circular passages. Also included in this study are the commonly-used geometries of rectangular passages.

Table 2
Comparison of data from Eqs. (27) and (29) with the exact series solutions of local and average Nusselt numbers for flow through circular pipes

$\hat{x}(a/D_h)^2$	Nu_D [9]	Nu_D Eq. (27)	ε Eq. (20)	$\overline{Nu}_D$ [9]	$\overline{Nu}_D$ Eq. (29)	ε Eq. (20)
5E–07	129.74	134.5	3.692	204.34	202.4	−0.976
1E–06	106.08	106.5	0.443	160.47	160.4	−0.059
2E–06	84.334	84.35	0.024	127.05	127.1	0.013
5E–06	61.877	61.88	0.008	93.334	93.34	0.012
0.00001	48.914	48.91	−0.004	73.869	73.87	0.009
0.00002	38.637	38.63	−0.028	58.429	58.43	0.000
0.00005	28.254	28.23	−0.085	42.812	42.80	−0.024
0.0001	22.279	22.24	−0.157	33.810	33.79	−0.059
0.0002	17.559	17.52	−0.245	26.683	26.65	−0.111
0.0005	12.824	12.77	−0.413	19.501	19.46	−0.217
0.001	10.130	10.08	−0.533	15.384	15.34	−0.310
0.002	8.0362	7.989	−0.589	12.152	12.10	−0.411
0.005	6.0015	5.979	−0.373	8.9432	8.903	−0.453
0.01	4.9161	4.924	0.153	7.1552	7.132	−0.326
0.02	4.1724	4.206	0.805	5.8146	5.815	0.002
0.05	3.7100	3.710	0.011	4.6406	4.655	0.302
0.10	3.6581	3.657	−0.036	4.1556	4.159	−0.104
0.20	3.6568	3.657	0.000	3.9063	3.908	0.231
0.50	3.6568	3.657	0.000	3.7566	3.757	3.279
1.00	3.6568	3.657	0.000	3.7067	3.707	5.874

2.2. Application to circular pipes

Using the above Airy equation analysis, Nusselt numbers for laminar flow through circular pipes are derived in this section. For hydrodynamically fully-developed flow through circular pipes with radius r_o, the velocity function after transforming the radial coordinate r by the relation $y = r_o - r$ is

$$\frac{u}{U} = 2\left[2\left(\frac{y}{r_o}\right) - \left(\frac{y}{r_o}\right)^2\right] \tag{25a}$$

with velocity slope at the wall

$$\left.\frac{du}{dy}\right|_{y=0} = 4\frac{U}{r_o} \tag{25b}$$

and therefore, $C = 4U/r_o$. According to Eq. (14b), the small x-solution for laminar and hydrodynamically fully-developed flow through circular ducts yields

$$Nu_D = \frac{1.709}{(\hat{x})^{1/3}}. \tag{26a}$$

with $\hat{x} = (x/r_o)/(Ur_o/\alpha)$. The deviation of this equation from the exact series solution [9] is plotted in Fig. 3, using dash lines with diamond shaped symbols. Although at very small values of $\hat{x}$ the error is relatively small, it begins to increase and then decrease as $\hat{x}$ increases. It is likely that the curvature effect begins to influence the velocity field as $\hat{x}$ increases. Assuming $(\hat{x})^{1/3}$ represents the first term in the Taylor series expansion of the temperature penetration; the next higher term must have the form $(\hat{x})^{2/3}/2!$ to be multiplied by an empirical factor of 4/3. Therefore, the

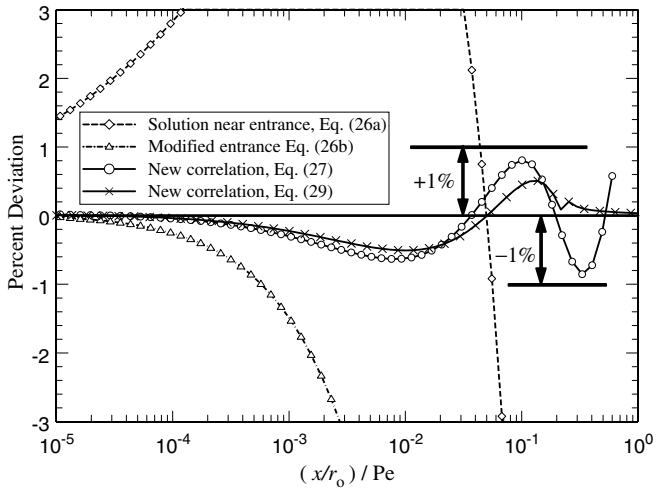

Fig. 3. Percent deviations for near entrance solutions, Eqs. (26a) and (26b), and for new correlations for Nu_D, Eq. (27), and $\overline{Nu}_D$, Eq. (29), as a function of $\hat{x}$ for flow in circular pipes.

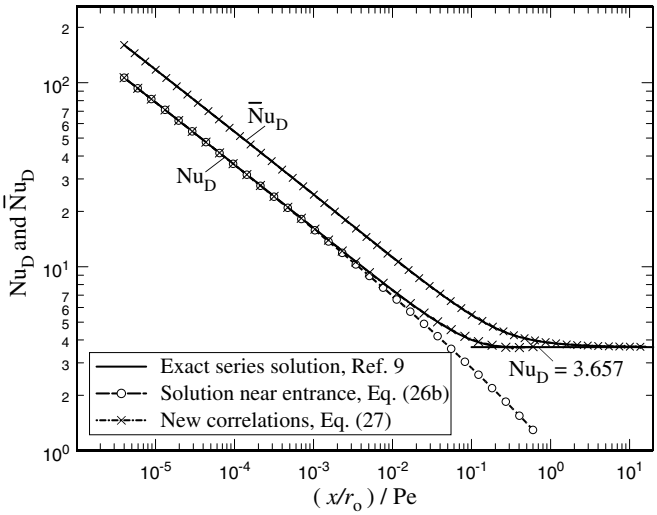

Fig. 4. A comparison of the Nusselt numbers from small-x solution, this new correlation, Eq. (27), and the exact series solution for laminar flow through circular pipes.

Nusselt number at small x values, is obtainable from the relation

$$Nu_D = \frac{1.709}{(\hat{x})^{1/3} + \frac{2}{3}(\hat{x})^{2/3}}, \tag{26b}$$

and it is to be examined. The data presented, in Fig. 3 by dot dash with triangular symbols show acceptable behaviors. Assuming Eq. (26b) to represent the solution at small values of $\hat{x}$, a correlation is prepared for the Nusselt number that emphasizes the small-x solution for the intermediate values of $\hat{x}$, it is

$$\begin{aligned} Nu_D &= \frac{hD_h}{k} \\ &= \frac{1.709}{(\hat{x})^{1/3} + \frac{2}{3}(\hat{x})^{2/3}} + \frac{3.657}{(1 + 1.86\hat{x}^{-3/2})^{4/15}} \quad \text{when } 0 \leqslant \hat{x} \leqslant 0.25 \\ &= 3.657 \quad \text{when } 0.25 < \hat{x} < \infty \end{aligned} \tag{27}$$

The data in Fig. 3 show that the deviation between data from Eq. (27) and those from [9] is within the targeted accuracy of less than 1%. As before, Table 2 is prepared to show a sample of acquired data and their comparison with those from [9]. Also, the substitution of Nu_D from Eq. (27) in Eq. (22) provides the average Nusselt number $\overline{Nu}_D = \bar{h}D_h/k$. Following the substitution, the resulting relation has an exact integral form

$$\begin{aligned} \overline{Nu}_D = 7.6905 &\left[\frac{1}{\hat{x}^{2/3}} - \frac{3\ln(1 + 2\hat{x}^{1/3}/3)}{2\hat{x}}\right] + \frac{2.61214}{(1 + 93x^{-3/2}/50)^{4/15}} \\ &\times \left\{(1 + 50\hat{x}^{3/2})^{4/15} \times {}_2F_1\left[\frac{14}{15}, \frac{4}{15}, \frac{29}{15}, -\left(\frac{50}{93}\right)\hat{x}^{3/2}\right]\right\} \\ &\text{when } 0 \leqslant \hat{x} \leqslant 0.25 \end{aligned} \tag{28a}$$

and

$$\overline{Nu}_D = 3.657 + \frac{0.2008}{\hat{x}} \quad \text{when } 0.25 < \hat{x} < \infty \tag{28b}$$

However, a simpler approximation with a comparable accuracy of less than 1% is

$$\begin{aligned} \overline{Nu}_D &= \frac{3.657}{(1 + 1.02\hat{x}^{-0.52})^{0.95}} + \frac{7.691}{\hat{x}^{2/3}} - \frac{11.536}{\hat{x}}\ln(1 + 2\hat{x}^{1/3}/3) \\ &\text{when } 0 \leqslant \hat{x} \leqslant 0.25 \\ &= 3.657 + \frac{0.2008}{\hat{x}} \quad \text{when } 0.25 < \hat{x} < \infty \end{aligned} \tag{29}$$

Fig. 4 compares the dot dash lines representing Eq. (29) with that from the exact series solution. The deviation between these two sets of data are graphically indistinguishable. Fig. 3 shows the deviation over the entire range of data from 0 to ∞ with deviations of less than 0.6%.

2.3. Application to rectangular ducts

The application of this small-x solution to rectangular passages is an important example, which can provide insight for extending the analysis to other applications. See Fig. 5 for the geometry of the cross-section with the width of $2a$ in the y-direction and $2b$ in the z-direction. In this problem, all the variables cannot be separated and the acquisition of an accurate exact solution at small values of x can be difficult. However, the small-x analysis in this paper is relatively straightforward, simple and accurate. As in the previous cases, in the small-x region, only the thin film next to the walls is relevant. The films near $y = \pm a$ and $z = \pm b$ are considered separately. Consider the surface at $y = a$. In the thin film near this surface, the velocity gradient is nearly linear in the y-direction and is modeled using $C_y(z)$ because it varies in the z-direction. Likewise, at the $z = b$ surface, the velocity gradient is $C_z(y)$. Consequently, the complex 3D heat transfer problem in the x-, y- and z-directions is reduced to two simpler 2D problems; one of these is for the $y = \pm a$ surfaces which

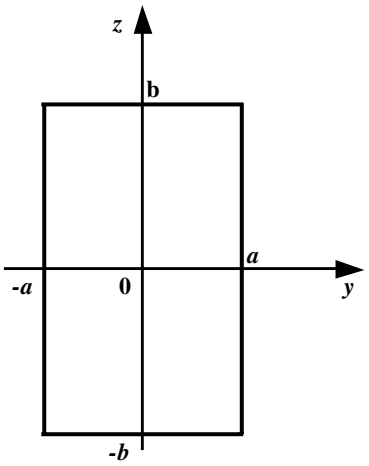

Fig. 5. Coordinates locations and dimensions for rectangular ducts.

is modeled as a partial differential equation in the y- and x-directions and the other is for the $z = \pm b$ surfaces which has a partial differential equation involving the z- and x-directions.

The 3D energy equation for hydrodynamically fully-developed flow and in the absence of axial conduction is

$$\frac{\partial^2\theta}{\partial\bar{y}^2}+\frac{\partial^2\theta}{\partial\bar{z}^2}=\left(\frac{u}{U}\right)\frac{\partial\theta}{\partial\hat{x}} \tag{30a}$$

The solution of Eq. (30a) when $\theta = 1$ at the walls and $\theta = 0$ when $\hat{x} = 0$ is given in [10]. This solution is obtained for relatively large x-values using the Green's function solution method in [11]. The computed series solution data [10], in Fig. 6, behaves well when $\hat{x} > 10^{-3}$ and they begin to fluctuate at the lower values of $\hat{x}$, as expected.

In the present analysis, the thin film normal to wall condition allows Eq. (30a) to be broken into the two different problems

$$\frac{\partial^2\theta}{\partial\bar{y}^2}=\frac{C_y(z)a}{U}\bar{y}\frac{\partial\theta}{\partial\hat{x}} \tag{30b}$$

and

$$\frac{\partial^2\theta}{\partial\bar{z}^2}=\frac{C_z(y)b}{U}\bar{z}\frac{\partial\theta}{\partial\hat{x}} \tag{30c}$$

Although the gradient $C_y(z)$ is a function of z in Eq. (30b), the velocity varies much less in the z-direction in the film than it does in the y-direction. Hence, its dependence can be neglected in the solution, as is demonstrated in the correlations given below.

For a rectangular duct, shown in Fig. 5, the average velocity gradient is needed on the walls. Because u/U depends on $\bar{y} = y/a$ and $\bar{z} = z/a$, the exact series solution [10] is

$$\frac{u}{U}=\frac{2\bar{b}}{\pi}\frac{\sum_{n=1}^{\infty}F_n(z)\cos(\beta_n y/a)}{\sum_{n=1}^{\infty}\frac{\beta_n\bar{b}-\tanh(\beta_n\bar{b})}{\beta_n^5}} \tag{31a}$$

with $\beta_n = (n - 1/2)\pi$

$$F_n(z)=\frac{(-1)^{n-1}}{(2n-1)\beta_n^2}\left[1-\frac{\cosh(\beta_n z/a)}{\cosh(\beta_n\bar{b})}\right] \tag{31b}$$

and

$$U=\frac{8a^2}{\pi^2\mu}\left(\frac{-\partial p}{\partial x}\right)\sum_{n=1}^{\infty}\frac{\beta_n\bar{b}-\tanh(\beta_n\bar{b})}{(2n-1)^2\bar{b}\beta_n^3} \tag{31c}$$

where p is the mean pressure at a given x location.

Now, one needs to differentiate Eq. (31a) with respect to y and evaluate it at $y = -a$ to obtain

$$C_y(z)=\left.\frac{\partial u}{\partial y}\right|_{y=-a}=U\frac{2\bar{b}}{\pi a}\frac{\sum_{n=1}^{\infty}F_n(z)\beta_n\sin(\beta_n)}{\sum_{n=1}^{\infty}\frac{\beta_n\bar{b}-\tanh(\beta_n\bar{b})}{\beta_n^5}} \tag{32a}$$

Similarly, one can differentiate Eq. (31a) with respect to z and evaluate it at $z = -b$ to get

$$C_z(y)=\left.\frac{\partial u}{\partial z}\right|_{z=-b}=U\frac{2\bar{b}}{\pi}\frac{\sum_{n=1}^{\infty}\frac{(-1)^n\tanh(\beta_n\bar{b})\cos(\beta_n y/a)}{(2n-1)\beta_n^2 a}}{\sum_{n=1}^{\infty}\frac{\beta_n\bar{b}-\tanh(\beta_n\bar{b})}{\beta_n^5}} \tag{32b}$$

Following the substitution of $C_y(z)$ from Eq. (32a) in Eq. (14b), it is to be integrated from $z = -b$ to b. This procedure is repeated after the substituting of $C_z(y)$ from Eq. (32b) in Eq. (14b) and integrating the resulting equation from $y = -a$ to a. The summation of these two quantities is divided $2a + 2b$ to get the average heat flux; that is,

$$q_{\mathrm{av}}(x)=-\frac{1}{2a+2b}\left\{\int_{-b}^{b}\frac{k(T_{\mathrm{w}}-T_{\mathrm{i}})}{\Gamma(2/3)}\frac{Ai'(0)}{Ai(0)}\left(\frac{C_y(z)}{\alpha x}\right)^{1/3}\mathrm{d}z+\int_{-a}^{a}\frac{k(T_{\mathrm{w}}-T_{\mathrm{i}})}{\Gamma(2/3)}\frac{Ai'(0)}{Ai(0)}\left(\frac{C_z(y)}{\alpha x}\right)^{1/3}\mathrm{d}y\right\} \tag{33}$$

However, due to symmetry conditions, this equation becomes

$$q_{\mathrm{av}}(x)=-\frac{1}{a+b}\frac{k(T_{\mathrm{w}}-T_{\mathrm{i}})}{\Gamma(2/3)}\frac{Ai'(0)}{Ai(0)}\left(\frac{U}{\alpha a x}\right)^{1/3}\times\left\{\int_0^b[aC_y(z)/U]^{1/3}\mathrm{d}z+\int_0^a[aC_z(y)/U]^{1/3}\mathrm{d}y\right\} \tag{34}$$

This definition of average heat flux introduces an equivalent $\overline{C}$,

$$(\overline{C})^{1/3}=\frac{1}{a+b}\left\{\int_0^b[aC_y(z)/U]^{1/3}\mathrm{d}z+\int_0^a[aC_z(y)/U]^{1/3}\mathrm{d}y\right\}, \tag{35}$$

that is needed for the computation of local heat transfer coefficient at any small $\hat{x}$ location from Eq. (14b); that is,

$$\frac{hD_{\mathrm{h}}}{k}=-\left(\frac{D_{\mathrm{h}}}{a}\right)\frac{(\overline{C})^{1/3}}{\Gamma(2/3)}\frac{Ai'(0)}{Ai(0)}\left(\frac{Ua^2}{\alpha x}\right)^{1/3}\frac{1}{1-\theta_{\mathrm{b}}} \tag{36}$$

Near the entrance location, θ_{b} in Eq. (36) becomes negligible and can be removes from Eq. (36).

Table 3 shows the values of $\overline{C}$ for rectangular ducts with different aspect ratios $\bar{b} = b/a$, for prescribed temperature

Table 3
Effective values of $\overline{C}$, Eq. (34), for rectangular ducts and prediction of Nu_D at $\hat{x} = 0.001$.

b/a	$aC_y(0)/U$	$aC_z(0)/U$	$\overline{C}$	Nu_D‡, Eq. (36)	Nu_D‡, Eq. (37)
1	4.804	4.804	3.325	16.07	15.01
1.2	4.567	4.250	3.069	17.07	16.06
1.5	4.329	3.719	2.866	18.35	17.40
2	4.067	3.233	2.731	20.07	19.20
3	3.742	2.819	2.689	22.46	21.69
4	3.550	2.644	2.711	24.02	23.31
5	3.430	2.549	2.739	25.11	24.44
6	3.352	2.489	2.766	25.91	25.27
7	3.297	2.448	2.788	26.52	25.90
8	3.256	2.418	2.807	27.00	26.40
9	3.226	2.395	2.823	27.39	26.80
10	3.202	2.377	2.837	27.71	27.15
15	3.132	2.325	2.883	28.73	28.20
20	3.098	2.300	2.909	29.28	28.76

‡ When $\hat{x} = 0.001$.

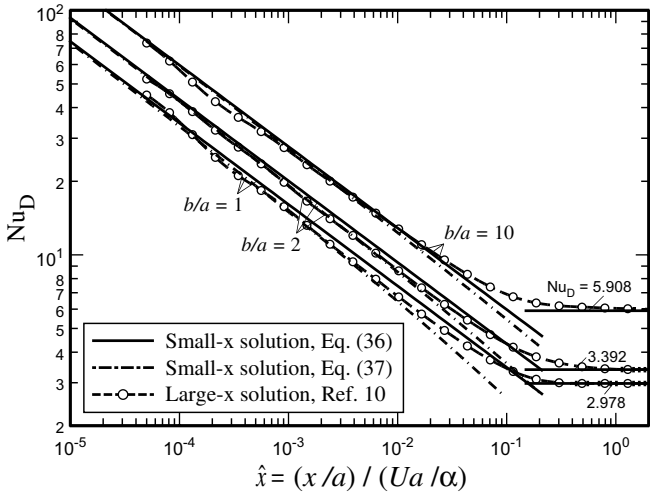

Fig. 6. A comparison between the small-x solutions, Eqs. (36) and (37), and the large-x solution, by the weighted residual method [10], for flow through rectangular ducts.

at the boundary. Also, for comparison, it includes the values of $aC_y(0)/U$ and $aC_z(0)/U$. As expected, for ducts with large aspect ratios, $aC_y(0)/U$ approaches 3 as given by Eq. (16) for parallel plate ducts. Using the data in [10], when $\hat{x} = 0.001$, the Nusselt number $Nu_D = hD_h/k$ values are 15.08, 18.92, and 26.37 when $\bar{b} = 1, 2$, and 10, respectively. For comparison, the corresponding values, using Eq. (36) with $\theta_b = 0$, are $Nu_D = 16.07$, 20.07, and 27.37. Using a modified form of Eq. (36), the computed Nusselt numbers are $Nu_D = 15.01$, 19.20, and 27.14 obtained from the equation

$$\frac{hD_h}{k} = \left(\frac{D_h}{2a}\right)\frac{1.0767(\overline{C})^{1/3}}{(\hat{x})^{1/3}[1+\gamma(\hat{x})^{1/3}]} \tag{37}$$

The parameter γ is computed using a simple interpolation; that is

$$\gamma = 0.151 + \frac{0.58}{\bar{b}} \tag{38}$$

The empirically determined values of γ are between those for the parallel plate channels and circular pipes. As $b/a \to \infty$, the parameter approaches 0.151. Also, when $b/a = 1$, the value of γ should be ~0.731 due to curvature effect within the temperature solution, similar to that for the circular pipe in Eq. (26b). For other aspect ratios, the Nusselt number when $\hat{x} = 0.001$ are also listed in Table 3. A comparison of these two sets of data indicates a small but significant improvement in the accuracy.

Fig. 6 shows the general behaviors of these solutions for rectangular ducts where hD_h/k is plotted as a function of $(x/a)/(Ua/\alpha) = (x/a)/Pe$ for different b/a values. The solid lines represent the computed data using Eq. (36). These are compared with the dash lines with circular symbols for the large-x solution; obtained using the extended weighted method in [10,11]. The data behavior is similar to those for the parallel plate channels and circular pipes. Furthermore, the study of expected improvement using Eq. (37) is an interesting feature of this small-x solution. The dot-dash lines in Fig. 6 are the solution using Eq. (37) and indeed they improved the accuracy of the small-x solution when b/a is small, as can be seen for $b/a = 1$ and 2. However, this figure shows that the effect of γ parameter, for $b/a = 10$, becomes relatively small, as was observed for parallel plate channels. Fig. 6 shows that the large-x solutions agree well with the solutions using Eq. (37) in the neighborhood of $\hat{x} = 10^{-3}$. At the larger $\hat{x}$ values, the small-x solutions begin to deviate, as expected. However, when $\hat{x} < 10^{-3}$, the large-x solutions show fluctuations due to the convergence characteristic of the series solution. This significant because it indicates a need for a relatively accurate solution as $\hat{x}$ becomes very small. Another point is the current Airy analysis again provides the simple dependence on the entrance distance (for small values) of x to the $-1/3$ power.

The form of Eq. (37) is similar that for cylinder, Eq. (26b). However, the parameter γ in Eq. (37) changes as b/a changes. It is possible to use a similar procedure to acquire a correlation for determining the heat transfer coefficient in rectangular ducts with uniform wall temperatures. The following relation produces reasonably accurate but with larger errors than those for parallel plate channels and circular pipes

$$Nu_D = \frac{hD_h}{k} = \left(\frac{D_h}{2a}\right)\frac{1.0767(\overline{C})^{1/3}}{(\hat{x})^{1/3}[1+\gamma(\hat{x})^{1/3}]} + \frac{0.75(Nu_D)_{FD}}{(1+\psi\hat{x}^{-3/2})^{1/3}}$$

$$\text{when } 0 \leqslant \hat{x}(a/D_h) \leqslant 0.3$$

$$= (Nu_D)_{FD} \quad \text{when } 0.3 < \hat{x}a/D_h < \infty \tag{39a}$$

where

$$\psi = \frac{(5+\bar{b})(1-\gamma)}{b(4+b)\gamma^{4/3}} \tag{39b}$$

and $(Nu_D)_{FD}$ is the Nusselt number for thermally fully-developed flow and it is presented in Table 4. Also, Table 4 contains the parameter ψ. Fig. 7 compares the Nusselt number values from Eq. (39a) with those from a large-x series solution, obtained using the technique in [10]. Both solutions agree well at the midrange but the series begins to show the sign of instability when $(x/a)/(Re_D Pr)$ is less than 10^{-3}.

The form of Eq. (39a) and the constant ψ are selected so that one can determine the average Nusselt number analytically since

$$I_1 = \int_0^{\hat{x}} \left(\frac{D_h}{2a}\right) \frac{1.0767(\overline{C})^{1/3}}{(\hat{x})^{1/3}[1+\gamma(\hat{x})^{1/3}]} = \left(\frac{D_h}{2a}\right) \frac{3.23(\overline{C})^{1/3}}{\gamma^2}\left\{\gamma(\hat{x})^{1/3} - \ln[1+\gamma(\hat{x})^{1/3}]\right\} \tag{40a}$$

$$I_2 = \int_0^{\hat{x}} \frac{0.75(Nu_D)_{FD}}{(1+\psi\hat{x}^{-3/2})^{1/3}}\,d\hat{x} = 0.75(Nu_D)_{FD}\left[(\psi+\hat{x}^{3/2})^{2/3} - \psi^{2/3}\right] \tag{40b}$$

and then

Table 4
Parameters in the Nusselt number correlations for rectangular ducts

b/a	$(Nu_D)_{FD}$	γ, Eq. (38)	ψ, Eq. (39b)	ω, Eq. (40d)
1.0	2.978	0.731	0.490	0.220
1.2	3.007	0.634	0.667	0.278
1.5	3.123	0.538	0.833	0.357
2	3.392	0.441	0.971	0.446
3	3.958	0.344	1.035	0.518
4	4.441	0.296	1.004	0.531
5	4.828	0.267	0.947	0.532
6	5.138	0.248	0.887	0.535
7	5.389	0.234	0.829	0.542
8	5.594	0.223	0.775	0.554
9	5.764	0.215	0.727	0.571
10	5.908	0.209	0.633	0.590

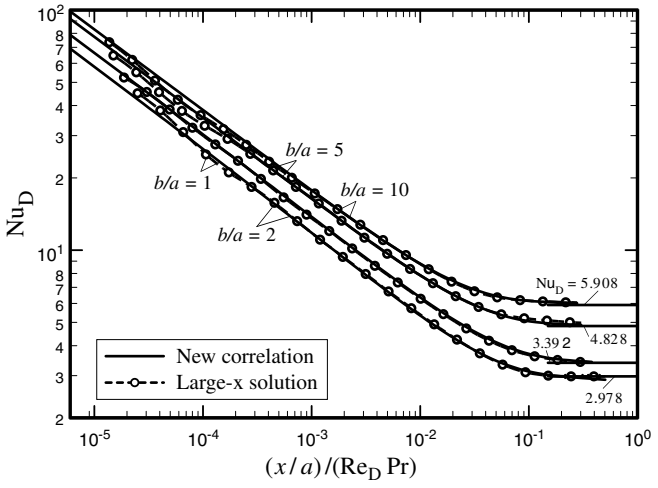

Fig. 7. A comparison of a small-x based new correlation, Eqs. (39a) and (39b), and exact large-x solution, as given in [10,11].

$$\overline{Nu}_D(\hat{x}) = \frac{1}{\hat{x}}[I_1(\hat{x}) + I_2(\hat{x})] \quad \text{when } 0 \leqslant \hat{x} \leqslant 0.3(D_h/a)$$
$$= (Nu_D)_{FD} + \frac{\omega}{\hat{x}} \quad \text{when } 0.3(D_h/a) < \hat{x} < \infty \tag{40c}$$

wherein ω is the value of

$$\omega = \left[\overline{Nu}_D(\hat{x})\big|_{\hat{x}=0.25(D_h/a)} - (Nu_D)_{FD}\right] \times 0.3(D_h/a) \tag{40d}$$

and its numerical values for different aspect ratios are in Table 4.

3. Discussion

As the entrance distance x becomes very small, the series solutions [10,11] for the temperature converge very slowly indeed. For example, for a Graetz type solution, over 500 eigenvalues may be needed at extreme accuracy for the determination of eigenfunctions. However, as x becomes small, the physical problem changes and permits an alternative and complementary analysis. As the series solution becomes more difficult and less accurate, this alternative solution becomes more accurate. Moreover, this paper shows that the dependence of h upon x for small dimensionless values is to the $-1/3$ power for a variety of cross-sections.

A combination of the small-x solution and large-x solution can serve as a useful tool to get accurate heat transfer data over the entire length of a duct. The methodology presented in the earlier sections was for the step change in the wall temperature. This type of solution can be extended to include other boundary conditions. For the case of constant heat flux the parallel plate channels are the primary candidates for illustrating the mathematical procedure. This is achievable by solving the Airy differential equation, Eq. (8), with prescribed heat flux at the wall, instead of temperature.

The solution procedure is similar to that for constant wall temperature case. Minor changes are needed such as having a new definition for dimensionless temperature

$$\Phi(x,y) = \frac{T(x,y) - T_i}{q_w a/k}, \tag{41a}$$

and the wall condition

$$-k\left.\frac{\partial T}{\partial y}\right|_{y=0} = q_w. \tag{41b}$$

Following the application of Laplace transform and utilization of Eq. (6), Eq. (8) takes the following form

$$\frac{\partial^2\bar{\Phi}(\eta)}{\partial\eta^2} = \eta\bar{\Phi}(\eta) \tag{42a}$$

with the boundary conditions

$$\left.\frac{d\bar{\Phi}}{d\eta}\right|_{\eta=0} = -\frac{1}{s^{4/3}}\left(\frac{\alpha}{Ca^3}\right)^{1/3} \quad \text{and} \quad \bar{\Phi}(\infty) = 0 \tag{42b}$$

Since $\bar{\Phi}(\infty) = 0$, the solution is $\bar{\Phi}(s,\eta) = C_1 Ai(\eta)$ and the second boundary condition yields the value of C_1, therefore,

$$\bar{\Phi}(s,\eta) = -\frac{1}{s^{4/3}}\left(\frac{\alpha}{Ca^3}\right)^{1/3}\frac{Ai(\eta)}{Ai'(0)} \tag{43}$$

At the wall, $\eta = 0$ and the inverse Laplace transform yields the wall temperature

$$\Phi(x,0) = -\frac{1}{\Gamma(4/3]}\left(\frac{\alpha x}{Ca^3}\right)^{1/3}\frac{Ai(0)}{Ai'(0)} = 1.5361\left(\frac{\alpha x}{Ca^3}\right)^{1/3} \tag{44}$$

and when $C = 3$, it becomes $\Phi(\hat{x},0) = 1.0651(\hat{x})^{1/3}$. Finally, the heat transfer coefficient is

$$\frac{h(2a)}{k} = \frac{2}{\Phi(x,0)} = \frac{2}{1.0651(\hat{x})^{-1/3}} = \frac{1.878}{(\hat{x})^{-1/3}} \tag{45}$$

which can be compared with Eq. (19a). Again, it has the same functional form.

An alternative method is to account for the wall temperature change using the Duhamel's theorem

$$T - T_i = \int_{\xi=0}^{\hat{x}}\left(\frac{dT_w(\xi)}{d\bar{x}}\right)\theta(\bar{y},\bar{x}-\xi)\,d\xi \tag{46}$$

where θ represents a temperature field following a wall temperature change equal to 1. Since the bulk temperature value is $T_b - T_i = (q_w a/k)\hat{x}$ and using $\Phi_w = (T_w - T_i)/(q_w a/k)$, then,

$$\hat{x} = \int_{\xi=0}^{\hat{x}}\left(\frac{d\Phi_w(\xi)}{d\xi}\right)H(\hat{x}-\xi)\,d\xi \tag{47a}$$

where

$$H(\hat{x}-\xi) = \int_0^1\left(\frac{u}{U}\right)\theta(\bar{y},\hat{x}-\xi)\,d\bar{y} \tag{47b}$$

has the value of $H(x-\xi) \cong \overline{C}\delta_t^2(x-\xi)/10$ with $\delta_t \cong (22.5\hat{x}/\overline{C})^{1/3}$ when using boundary layer analysis. The solution of Eq. (47a) following a standard Laplace transform procedure is

$$\Phi_w(\hat{x}) = \left(\frac{2}{3}\right)^{5/3}\frac{(15/\overline{C})^{1/3}\hat{x}^{1/3}}{\Gamma(5/3)\Gamma(4/3)} = 1.5565\left(\frac{\hat{x}}{\overline{C}}\right)^{1/3} \tag{48}$$

For parallel plate channels, $\overline{C} = 3$ and $\Phi_w(\hat{x}) = 1.0792\hat{x}^{1/3}$; the coefficient 1.0792 compares well with 1.0651 obtained from Eq. (44), with a factor or 1.013 as before. For $\hat{x} = 10^{-5}, 10^{-4}, 10^{-3}$, and 10^{-2}, Eq. (44) provides the Nusselt numbers $ha/k = 1/[\Phi_w(\hat{x}) - \hat{x}] = 43.58$, 20.23, 9.389, 4.358, at $\hat{x} = 10^{-5}, 10^{-4}, 10^{-3}$, and 10^{-2}, respectively. A large-x solution yields the corresponding values, $ha/k =$ 44.08, 20.19, 9.386, and 4.455, indicating deviations of 1.1%, 0.19%, 0.03%, 2.2%. As expected, the deviation is small at the midrange while, at $\hat{x} = 0.01$, the deviation becomes large because it is near the range of validity of the small-x solution. The larger deviation at $\hat{x} = 10^{-5}$ is caused by the numerical errors in large-x solution. Similarly, using Eq. (48), one obtains $ha/k = 43.03$, 20.00, 9.353, and 4.494 at $\hat{x} = 10^{-5}, 10^{-4}, 10^{-3}$, and 10^{-2} with respective errors of 2.4%, 0.95%, 0.35%, and 3.2%. This attests to the combined effects of the small-x and large-$x$solution as they can provide accurate data over the entire length of a duct.

4. Conclusions

An exact asymptotic solution is developed mainly to evaluate the heat transfer coefficient at very small distances from the thermal entrance location in a flow passage. It is demonstrated that this solution can be used to verify the accuracy of large-x solution as x reduces, as can be seen by examining the large-x solution in Fig. 6. Accurate analytical results at all values of x, from zero to infinity, with deviations of well below 1% are attainable for parallel plate channels, Fig. 2, and for circular pipes, Fig. 4. Modifications are also presented to extend this methodology to other passages, e.g., using rectangular ducts.

A very important point is that this method of solution for small x is general because it leads to simplified solutions for many cross-sectional shapes including flow in flat plates, rectangles, cylinders, annuli and others. By having this method of solution, many heat transfer problems of this type can be readily treated. Furthermore, considerable insight is obtained into the heat transfer in inlet regions. As an illustration, this analysis produced a simple analytical form that indicates the heat transfer coefficient h being proportional to $x^{-1/3}$ as x goes to zero while the series solutions do not show this behavior. Another significant point is that the solution for small x is complementary to series solution, because, it is valid just where the series solution begins to falter. In the region where both solutions are accurate, intrinsic verification [12] is possible. Having two solutions that provide about the same numerical values, but yet are completely different and independent, provides considerable confidence in both solutions.

References

[1] W.M. Kays, M.E. Perkin, Forced Convection, Internal Flow in Ducts, in: W.M. Rohsenow, J.P. Hartnett (Eds.), Handbook of Heat Transfer, McGraw-Hill, New York, 1973, Section 7.
[2] R.K. Shah, A.L. London, Laminar Flow Forced Convection in Ducts, in: Supplement 1 to Advances in Heat Transfer, Academic Press, New York, 1978.
[3] W.M. Kays, H.C. Crawford, Convective Heat and Mass Transfer, 3rd ed., McGraw-Hill, New York, 1993.
[4] L.C. Burmeister, Convective Heat Transfer, 2nd ed., Wiley, New York, 1993.
[5] A. Bejan, Convection Heat Transfer, 2nd ed., Wiley, New York, 1982.
[6] M. Abramowitz and I.A. Stegun, Handbook of Mathematical Functions, National Bureau of Standards Applied Mathematics Series 55, 1965.
[7] V.S. Arpaci, P.S. Larsen, Convection Heat Transfer, Prentice-Hall, New Jersey, 1984.
[8] J. Kestin, L.N. Persen, The transfer of heat across a turbulent boundary layer at very high Prandtl number, Int. J. Heat Mass Transfer 8 (3) (1962) 355–371.

[9] A. Haji-Sheikh, Estimation of average and local heat transfer in parallel plates and circular ducts filled with porous materials, J. Heat Transfer 126 (3) (2004) 400–409.
[10] A. Haji-Sheikh, D.A. Nield, K. Hooman, Heat transfer in the thermal entrance region for flow through rectangular porous passages, Int. J. Heat Mass Transfer 49 (17–18) (2006) 3004–3015.
[11] J.V. Beck, K. Cole, A. Haji-Sheikh, B. Litkouhi, Heat Conduction Using Green's Functions, Hemisphere Publ. Corp., Washington DC, 1992.
[12] J.V. Beck, R. McMasters, K.J. Dowding, D.E. Amos, Intrinsic verification methods in linear heat conduction, Int. J. Heat Mass Transfer 49 (17–18) (2006) 2984–2994.